Evolution of Amorphous Calcium Phosphate to Hydroxyapatite Probed by Gold Nanoparticles

ARTICLE *in* THE JOURNAL OF PHYSICAL CHEMISTRY C · SEPTEMBER 2008

Impact Factor: 4.77 · DOI: 10.1021/jp804371u

Article

Evolution of Amorphous Calcium Phosphate to Hydroxyapatite Probed by Gold Nanoparticles

Jinhui Tao, Haihua Pan, Jieru Wang, Jia Wu, Ben Wang, Xurong Xu, and Ruikang Tang

J. Phys. Chem. C, **2008**, 112 (38), 14929-14933• DOI: 10.1021/jp804371u • Publication Date (Web): 27 August 2008

Evolution of Amorphous Calcium Phosphate to Hydroxyapatite Probed by Gold Nanoparticles

Jinhui Tao,[†] Haihua Pan,[†] Jieru Wang,[‡] Jia Wu,[†] Ben Wang,[†] Xurong Xu,[†] and Ruikang Tang*,[†]

Department of Chemistry and Center for Biomaterials and Biopathways, Zhejiang University, Hangzhou, Zhejiang 310027, China, and Centers of Analysis and Measurement, Zhejiang University, Hangzhou, Zhejiang 310027, China

Received: May 17, 2008; Revised Manuscript Received: June 25, 2008

Amorphous calcium phosphate (ACP) is an important intermediate phase during the biomineralization of apatite. But the detailed mechanism of transformation from ACP to crystallized hydroxyapatite (HAP) is still unclear. Gold nanoparticles are used as *ex-situ* probes to monitor the detailed evolution process of ACP *in vitro*. The rearrangement of gold nanoparticles during the evolution of ACP indicates the aggregation and surface-mediated crystallization subprocesses. The former process can be observed by the bottleneck-like connection and the distribution of gold nanoparticles inside the microspheres. After aggregation, surface-mediated crystallization dominated. The HAP nanoneedles first formed at the ACP-solution interface and extended outward radially. In this process, the ACP microsphere provides a template and nutrient for the growth and assembly of HAP nanoneedles, which is consistent with the well-known modified Kirkendall process. Neither the dissolution−recrystallization process nor the internal rearrangement mechanism is applicable for the explanation of such phenomena. Accordingly, the aggregation and Kirkendall process coupled with surface crystallization are proposed for an alternative mechanism for the evolution of ACP into HAP probed by gold nanoparticles. Although biomineralization is a complicated process in the presence of numerous biomolecules, our conceptual mechanism, revealed by the gold probe, may be also applied to understand the phase transformation in living organisms. This study shows that the involvement of gold nanoparticles can provide a new strategy to investigate the detailed evolution process of amorphous materials.

Introduction

Amorphous materials represent about 25% of the minerals formed under the induction or control of living organisms.[1] Among these amorphous minerals are those that have similar chemical composition with different degrees of short-range order.[2,3] Amorphous calcium phosphates (ACP) have been widely regarded as the metastable precursor phase for the subsequent formation of thermodynamically more stable calcium phosphate phases such as octacalcium phosphate (OCP) and hydroxyapatite (HAP) depending on the pH value of the solution.[4−6] However, the detailed process during ACP-HAP conversion is still equivocal in spite of intensive efforts. Some authors have proposed that dissolution of ACP and nucleation and growth of HAP from solution is responsible for the phase transformation process,[2,7−9] while others consider the crystallization process as internal structure rearrangement.[4,10−12] Because of the difficulties in capturing intermediate states and precise monitoring of details during the evolution, both mechanisms have been proposed to explain the transformation. Herein, gold nanoparticles (Au NPs), which are chemically inert with respect to the surrounding solutions and can be distinguished easily from produced minerals, were used as the *ex-situ* probes to investigate the reaction. It was revealed that ACP-HAP conversion is aggregation and Kirkendall effect coupled with an interfacial reaction. Knowledge regarding the details of the mineral evolution process not only contributes to an understanding of how hard tissues are formed[9,13−16] but also acts to guide the design of biomaterials with excellent performance.[12,17,18]

2. Experimental Section

2.1. Materials. All reagents were of analytical grade and used without further purification. Triply distilled CO_2-free water was used in experiments. All solutions were filtered through 0.22 μm Millipore films prior to use.

2.2. Analytical Methods. TEM and SAED observations were performed by using a JEM-200CX (JEOL, Japan) transmission electron microscope at an acceleration voltage of 160 kV. HRTEM imaging were performed by using a JEM-2010HR (JEOL, Japan) high resolution TEM at an acceleration voltage of 200 kV. Scanning electron microscopy (SEM) was performed by using a S-4800 field-emission scanning electron microscope (HITACHI, Japan) at an acceleration voltage of 5 kV. The particle size distributions and average particle sizes were measured by using a laser light scattering spectrometer (Malvern, Zetasizer Nano-S, UK) with a He−Ne laser with an output wavelength of 633 nm. FTIR spectra (Nicolet, Nexus670, USA) were used for crystallinity identification. UV−vis absorption spectra were recorded by a UV-265 spectrophotometer (Shimadzu Corporation, Japan) to detect the aggregation state of gold nanoparticles and the presence of gold nanoparticles on the HAP dandelions.

2.3. Synthesis of Au Nanoparticles. Au NPs were prepared by citrate reduction of $HAuCl_4$ solutions. Typically, 1.67 mL of 1% (w/v) sodium citrate solution was added into 48.33 mL

* Corresponding author. Phone/Fax: +86-571-87953736. E-mail: rtang@zju.edu.cn.
[†] Department of Chemistry and Center for Biomaterials and Biopathways.
[‡] Centers of Analysis and Measurement.

10.1021/jp804371u CCC: $40.75
Published on Web 08/27/2008

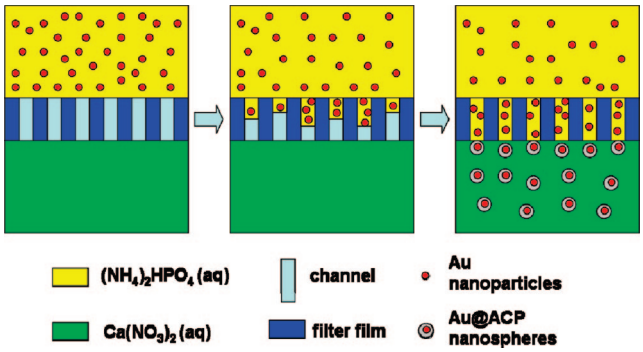

Figure 1. Schematic representation of the experimental setup. Gold probed $(NH_4)_2HPO_4$(aq) (4.05 mM) is diffused into $Ca(NO_3)_2$ (aq) (6.75 mM). Au@ACP particles are synthesized and were used for further monitoring the evolution process.

of $HAuCl_4$ boiling solution (0.44 mM). Within 5 min, the solution turned out to be wine-red, indicating the formation of Au NPs. After boiling for another 10 min, the dispersion was cooled down to room temperature (20 °C) in air. The Au NPs obtained were about 16 nm in size, determined by means of TEM and DLS. They exhibited a distinct surface plasmon absorption band, centered at 520 nm. In order to remove the capping agent citrate, 20 mL suspensions of gold nanoparticles were dialysized (Mw = 3500 Da) in 1 L water for 96 h at 37 ± 1 °C; water was changed for every 12 h. Finally, the dialysized Au colloid was further filtered through filter membranes (Millipore, 220 nm pore diameter) to remove a few aggregates after dialysis.

2.4. Evolution of ACP without the Addition of Au NPs. The concentrations of $Ca(NO_3)_2$ (aq) and $(NH_4)_2HPO_4$(aq) were 6.75 mM and 4.05 mM, respectively. The pH of both solutions was adjusted to 10.00 ± 0.05 by 25% (w/v) NH_4OH and then filtered through filter membranes (Millipore, 220 nm pore diameter) before use. The reaction was performed by the diffusion method: equal volume $(NH_4)_2HPO_4$(aq) solutions (5 mL) were distributed into three beakers with volumes of 50 mL, then equal volume $Ca(NO_3)_2$(aq) solutions (5 mL) were spontaneously diffused into 5 mL of $(NH_4)_2HPO_4$(aq) solutions through the above-mentioned filter membranes at the temperature of 37 ± 1 °C. At different reaction times, 2.5 h, 5 h, and 12 h, a beaker was removed, and the precipitate was collected by centrifugation at 2700g for 3−5 min. The solids were washed several times with deionized water and were vacuum-dried at 37 ± 1 °C.

2.5. Au@ACP Core−Shell Structure and Its Evolution. In order to investigate the aggregation and subsequent evolution process, 1 mL of $(NH_4)_2HPO_4$(aq) (81 mM) solution was diluted in the above dialyzed and filtered Au colloids (19 mL) to form a solution with the same phosphate concentration (4.05 mM), and the pH of this solutions was adjusted to 10.00 ± 0.05 by 25% (w/v) NH_4OH. Then this solution was used as the phosphate source and the experiments repeated. As the gold nanoparticles passed through the filter membranes (Millipore, 220 nm pore diameter) from $(NH_4)_2HPO_4$ (4.05 mM) solution to $Ca(NO_3)_2$ (6.75 mM) solution, the nucleation events at the gold surface took place resulting in the formation of Au@ACP core/shell-type nanospheres within 16 min. Au@ACP nanospheres synthesized at 2.5 h were collected by centrifuging at 2700g for 3−5 min, then were washed and redispersed into the mother liquor corresponding to 2.5 h in part 2.4, which were transformed for another 9.5 h. The schematic diagram of the setup adopted in this study is presented in Figure 1.

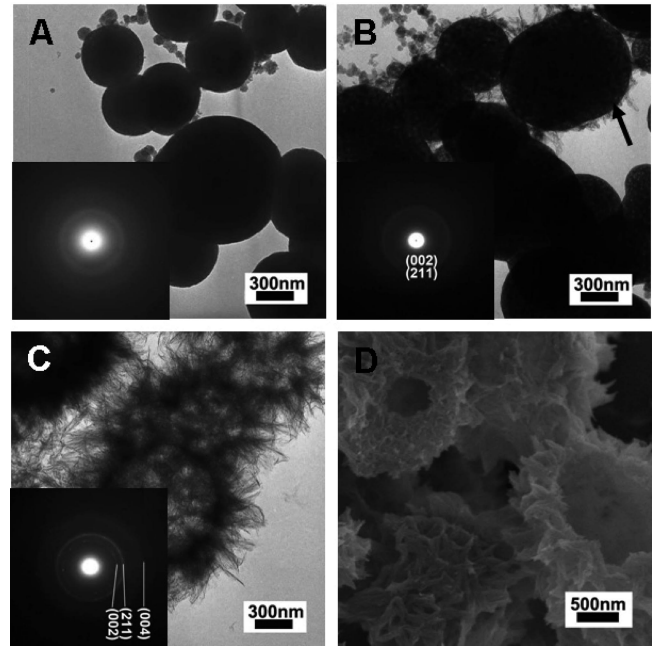

Figure 2. TEM and SEM images of calcium phosphates at the different stages of evolution in the absence of gold nanoparticles. (A) 2.5 h; (B) 5 h; (C) 12 h; (D) SEM image of cracked dandelions at 12 h.

2.6. Au Coated ACP Microspheres and Evolution. In order to explore the details of interfacial transformation, the sample synthesized at 2.5 h according to part 2.4 was collected and washed by water several times, then was dispersed in the dialyzed and filtered Au suspensions for 10 min. Afterward, the Au coated ACP microspheres were gathered by centrifuging at 2700g for 3−5 min, then were washed several times to remove the unabsorbed Au nanoparticles. The samples were redispersed into the mother liquor corresponding to 2.5 h. The Au coated ACP microspheres were further transformed for another 2.5 and 9.5 h.

3. Results and Discussion

In the system without the addition of gold probes, the products at 2.5 h were still amorphous as indicated by the diffusive diffraction rings under the selected area electron diffraction (SAED, Figure 2A) and FTIR spectrum (Figure S1, Supporting Information). The crystallized tinny nanoneedles grew from the surface of certain ACP microspheres at 5 h (Figure 2B). The low crystallinity of these nanoneedles was indicated by the weak intensity of the diffraction rings in the SAED pattern. In this stage, the size and shape of the ACP core were still preserved, which indicated that the dissolution process was negligible. The surface of the ACP core serves asthe nucleation site for HAP nanoneedles. HAP dandelions with greater sizes (diameters up to 2−3 μm) formed after reaction for 12 h. These dandelions were constructed by the assembly of numerous nanoneedles. The width and length of these nanoneedles are in the range of 10−30 nm and 600−800 nm (Figure 2C), which had an improved crystallinity as seen by the inset SAED pattern and FTIR spectra (Figure S1, Supporting Information), Individual HAP nanoneedles are single crystalline, as revealed in the HRTEM images and clear lattice fringes of (002) and (300) (Figure S2B, Supporting Information). The long axis of the nanoneedles is along the [001] orientation, and the hollow nature of dandelion was further clarified by the SEM image of cracked dandelions (Figure 2D).

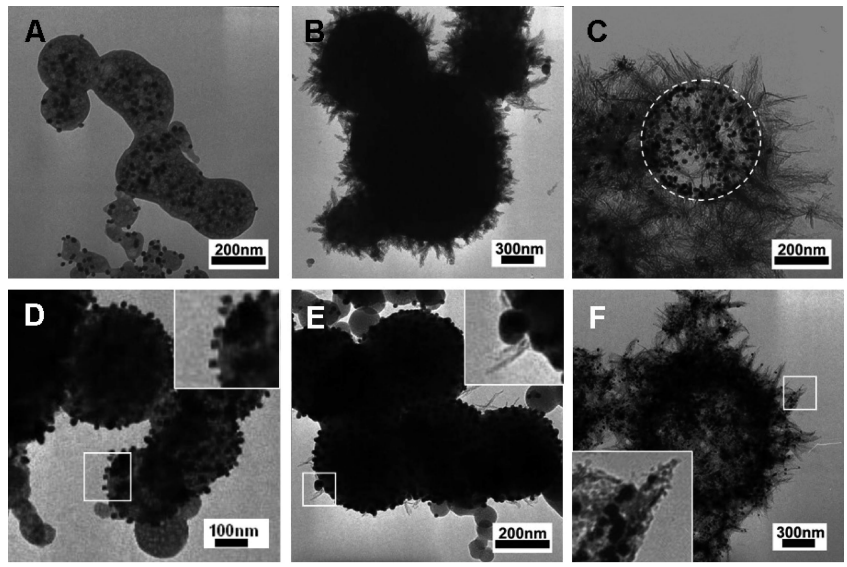

Figure 3. TEM images of calcium phosphates at different intervals in the presence of gold nanoparticles. (A−C) Gold nanoparticles were immersed into calcium phosphates. (A) 16 min; (B) 5 h; (C) 12 h. (D−F) Gold nanoparticles were loaded on the surface of ACP microspheres. (D) 2.5 h; (E) 5 h; (F) 12 h. The inset figures are the enlargements of the regions in squares.

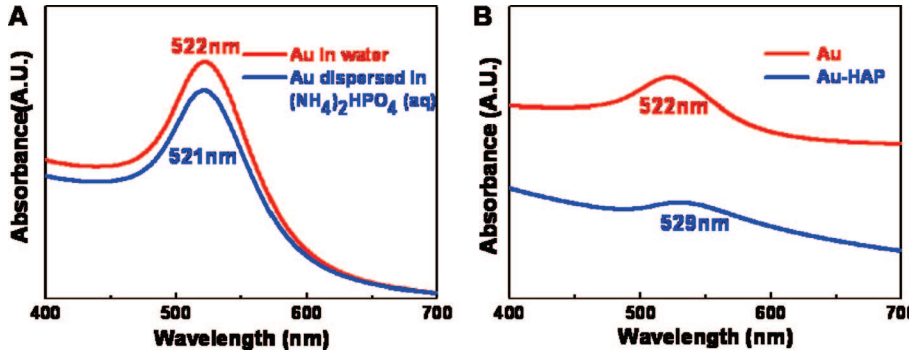

Figure 4. UV−vis absorption spectra of gold nanoparticles in the absence and presence of $(NH_4)_2HPO_4$ (A), and gold nanoparticles and gold-HAP dandelions (B). The spectral profile of the gold colloid was unchanged after the addition of $(NH_4)_2HPO_4$, which indicated that the size of Au NPs was sustained. While the gold nanoparticles were immobilized on the surface of HAP aggregates, the red-shift (~7 nm) of the surface plasmon absorption band was observed, which may originate from Au-HAP interfacial interaction.

The size distribution of gold nanoparticles before and after the addition of $(NH_4)_2HPO_4$ was unchanged as indicated by dynamic light scattering measurements (DLS, Figure S3, Supporting Information). The Au@ACP core−shell structure formed when the $(NH_4)_2HPO_4$ solution diffused into $Ca(NO_3)_2$ solution after reaction for 2.5 h. However, the primary nanospheres with one gold core could rarely be observed for rapid coalescence process, which was beyond the ability of *ex-situ* DLS techniques (Figure S4, Supporting Information). The self-aggregation of these primary particles can be proposed as most spheres contained more than one gold core when reaction for only 16 min (Figure 3A). After reaction for 12 h, the Au NPs remained on the internal wall of the HAP dandelions to form a spherical gold layer (Figure 3C). The diffusion coefficients of Au NPs inside ACP spheres were lower than that of ACP. The spherical shape of the gold layer demonstrated that the material flux inside the ACP spheres was isotropic, which is a property of amorphous materials.

We further investigated the mechanism of interfacial events by utilizing the Au NP probe. In this experiment, ACP spheres were first synthesized by diffusion reaction for 2.5 h, and their surfaces were coated by Au NPs. These gold coated ACP spheres were redispersed into the mother liquor corresponding to that of 2.5 h. The surface of ACP spheres was uniformly covered by the Au NPs as seen by TEM (Figure 3D). The HAP nanocrystals nucleated first at the gaps between two Au NPs after reaction for 5 h (Figure 3E). Finally, the interface of HAP/solution moved outward, and the Au NPs were pushed outside from the original location without being dispersed back into the bulk solution (Figure 3F). The Au NPs had adsorbed on the surface of HAP dandelions, and a red-shift of surface plasma resonance peak from 522 to 529 nm of Au was observed (Figure 4).

Clearly, Au NPs hadn't changed the pathway of transformation phenomenologically as the morphologies and phases at different stages were similar in the presence and absence of gold probes. The whole evolution process can be divided into two steps: (1) spontaneous aggregation. The aggregation could occur between nanospheres−nanospheres or nanospheres−microspheres (Figures S2A and S5, Supporting Information). This phenomenon could be explained by Ostwald ripening with particle coalescence to minimize the interfacial free energy.[19] (2) Kirkendall effect with interfacial reaction. The HAP nanoneedles nucleated at the ACP/solution interface and extended outward radially, while the internal ACP phase provided material flow flux for the phase conversion to HAP (Figures 3 and 5). The size and shape of the ACP core was well preserved as the reaction proceeds up until 5 h (Figures 2B and 3B and E). There was no noticeable dissolution of ACP before surface nucleation of hydroxyapatite. Thereafter, the ACP core eliminated as the

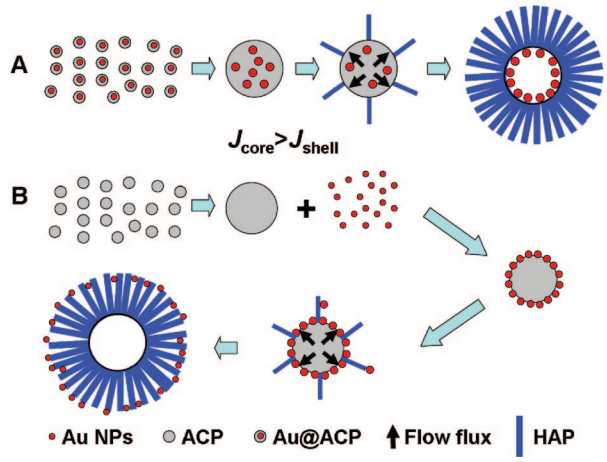

Figure 5. Schematic illustration of evolution of ACP probed by Au NPs (A) for self-aggregation and Kirkendall process or (B) the surface of ACP sphere solution-mediated interface reaction.

HAP dandelion grew, leaving a hollow core with a size similar to that of the former ACP core. As proposed by Smigelskas and Kirkendall,[20] if the mutual diffusion flux (J) of two components in a diffusion couple differs by a substantial amount, their interdiffusion at the interface may result in a net directional flow of matter. When the flux from core to shell (J_{core}) was much larger than that from shell to core (J_{shell}), the interface between core and shell moved outward from the core, leaving vacancies behind. More vacancies were generated and accumulated in the core to form a void until the reaction terminated (Figure 5).

The dissolution and recrystallization mechanism assumes that the transformation from ACP to HAP involves three basic steps: (1) the dissolution and hydration of ions from ACP; (2) the transfer of these hydrated ions; (3) the nucleation and subsequent growth of HAP.[9] This model is proposed on the basis of data of X-ray diffraction, IR spectroscopy, and chemical composition of solution and solids, without considering the microscopic details. However, in our experiments the hollow core of crystalline aggregates (Figure 2C and D) retained the size and shape of the ACP precursor. The spherical morphology can hardly be kept during the transfer of hydrated ions during the dissolution and renucleation processes without the involvement of a relatively stable ACP-HAP interface. Moreover, the gold probes on the surface of gold coated ACP microspheres finally existed only on the outer layer of HAP dandelions without coming back to the bulk solution. These Au NPs were inevitably dispersed into bulk solution as the complete dissolution of ACP and migration of hydrated ions proposed by the former model. The other prevailing internal rearrangement mechanism[10−12] said that the small essential particles in the solution are incorporated into the loose-structured amorphous aggregate with time. With the increase in the number of particles within the aggregate, the internal structure changes to closely packed to reduce the total free energy of the aggregate, resulting in HAP nucleation. This process can proceed via the assumption that the structure of ACP directly transforms to that of HAP by rearrangement of each molecule. This case indicates that ACP has structural resemblance to that of HAP and strongly supports that the basic growth unit of HAP is Posner's cluster similar to that of ACP.[2,11] Although the internal rearrangement may be applicable to explain the sustained morphology, the radial material flux was not revealed in this model. The hollow nature of HAP aggregates is against the former idea that the density of the internal part of ACP increases during the assimilation of growth units from solution. Although the Kirkendall effect has been used widely in the controlled synthesis of other hollow structured materials, such as CoO,[21] Fe_2O_3,[22] and ZnO,[23] it has not been elucidated during the phase transformation in biomineralization.

It has been reported that amorphous materials may have important basic functions in many biomineral formation processes as a transient precursor.[24,25] An amorphous mineral is isotropic and can be shaped more easily by the space in which it forms. The phase transformation of amorphous minerals in a confined space contributes to the formation of biominerals with complex shapes. However, in a biological system, organized biopolymers (such as protein and polysaccharides) or even cells and vesicles exert control over the site, structure, and orientation of inorganic nuclei as well as macroscopic arrangement of the minerals.[26] Biomineralization is a rather complicated process, and the formation of biogenic minerals cannot be attributed to one or several simple factors. Therefore, the proposed paradigm here is to be interpreted as a conceptual mechanism, and it may be also valid in the living systems. Further studies of the ACP phase transformation in the presence of biopolymers or even organisms need to be performed to gain deeper insight. The proposed aggregation and Kirkendall effect coupled with interfacial reaction model can be used as a simplified mechanism for explaining the formation of novel calcium phosphate morphology during the mineralization processes from the viewpoint of physical chemistry.[13−16,27−29]

4. Conclusions

In summary, gold NPs were used as *ex-situ* probes for the detection of transient and detailed processes during phase transformation from ACP to HAP by the diffusion method, which is a multistep process involving self-aggregation and the Kirkendall effect. The proposed model offers an alternative mechanism instead of conventional dissolution and recrystallization or internal rearrangement interpretations of evolution from ACP to HAP. We suggest that our experimental strategy may provide a novel technique to examine the phase transformation of biominerals in living organisms, which is a key issue in the current studies of biomineralization.

Acknowledgment. We thank Mr. Y. W. Wang for his assistances in the TEM characterizations. This work was supported by the National Natural Science Foundation of China (20601023 and 20571064), Zhejiang Provincial Natural Science Foundation of China (R407087), and Cheung Kong Scholars Program (RT).

Supporting Information Available: DLS and TEM of Au NPs and ACP, FTIR spectra, UV−vis data, and SEM images. This material is available free of charge via the Internet at http://pubs.acs.org.

References and Notes

(1) Weiner, S.; Dove, P. M. *Rev. Mineral. Geochem.* **2003**, *54*, 1–29.
(2) Posner, A. S.; Betts, F. *Acc. Chem. Res.* **1975**, *8*, 273–281.
(3) Betts, F.; Blumenthal, N. C.; Posner, A. S.; Becker, G. L.; Lehninger, A. L. *Proc. Natl. Acad. Sci. U.S.A.* **1975**, *72*, 2088–2090.
(4) Abbona, F.; Baronnet, A. *J. Cryst. Growth* **1996**, *165*, 98–105.
(5) Tung, M. S.; Brown, W. E. *Calcif. Tissue Int.* **1983**, *35*, 783–790.
(6) Brecevic, Lj.; F. .uredi-Milhofer, H. *Calcif. Tissue Int.* **1972**, *10*, 82–90.
(7) Boskey, A. L.; Posner, A. S. *J. Phys. Chem.* **1973**, *77*, 2313–2317.
(8) Lazic, S. *J. Cryst. Growth* **1995**, *147*, 147–154.
(9) Blumenthal, N. C.; Posner, A. S. *Calc. Tissue Res.* **1973**, *13*, 235–243.
(10) Onuma, K.; Ito, A. *Chem. Mater.* **1998**, *10*, 3346–3351.

(11) Onuma, K.; Oyane, A.; Tsutsui, K.; Tanaka, K.; Treboux, G.; Kanzaki, N.; Ito, A. *J. Phys. Chem. B* **2000**, *104*, 10563–10568.
(12) Onuma, K. *Prog. Cryst. Growth Charact. Mater.* **2006**, *52*, 223–245.
(13) Lowenstam, H. A.; Weiner, S. *Science* **1985**, *227*, 51–53.
(14) Lee, A. P.; Brooker, L. R.; Macey, D. J.; van Bronswijk, W.; Webb, J. *Calcif. Tissue Int.* **2000**, *67*, 408–415.
(15) Weiner, S. *Bone* **2006**, *39*, 431–433.
(16) Grynpas, M. D.; Omelon, S. *Bone* **2007**, *41*, 162–164.
(17) Onuma, K.; Kanzaki, N.; Kobayashi, N. *Macromol. Biosci.* **2004**, *4*, 39–46.
(18) Tao, J.; Pan, H.; Zeng, Y.; Xu, X.; Tang, R. *J. Phys. Chem. B* **2007**, *111*, 13410–13418.
(19) Madras, G.; McCoy, B. J. *J. Colloid Interface Sci.* **2003**, *261*, 423–433.
(20) Smigelskas, A. D.; Kirkendall, E. O. *Trans. AIME* **1947**, *171*, 130–142.
(21) Yin, Y.; Rioux, R. M.; Erdonmez, C. K.; Hughes, S.; Somorjai, G. A.; Alivisatos, A. P. *Science* **2004**, *304*, 711–714.
(22) Cabot, A.; Puntes, V. F.; Shevchenko, E.; Yin, Y.; Balcells, L.; Marcus, M. A.; Hughes, S. M.; Alivisatos, A. P. *J. Am. Chem. Soc.* **2007**, *129*, 10358–10360.
(23) Liu, B.; Zeng, H. C. *J. Am. Chem. Soc.* **2004**, *126*, 16744–16746.
(24) Politi, Y.; Arad, T.; Klein, E.; Weiner, S.; Addadi, L. *Science* **2004**, *306*, 1161–1164.
(25) Addadi, L.; Raz, S.; Weiner, S. *Adv. Mater.* **2003**, *15*, 959–970.
(26) Veis, A. *Rev. Mineral. Geochem.* **2003**, *54*, 249–289.
(27) Liu, J.; Wu, Q.; Ding, Y. *Eur. J. Inorg. Chem.* **2005**, *414*, 5–4149.
(28) Gajjeraman, S.; Narayanan, K.; Hao, J.; Qin, C.; George, A. *J. Biol. Chem.* **2007**, *2 82*, 1193–1204.
(29) Benzerara, K.; Menguy, N.; Guyot, F.; Skouri, F.; de Luca, G.; Barakat, M.; Heulin, T. *Earth Planet. Sci. Lett.* **2004**, *228*, 439–449.

JP804371U